Supplement to *A new global P-wave tomographic model of the Earth's mantle*, by G. Nolet et al.

Figs. S1-S10: Large scale versions of model UNICA25. We chose a variable colour scale (in %), such that the full colour scale corresponds to a temperature range of ±600°K as suggested by the compressional velocity derivatives $\mathrm{d}\ln V_P/\mathrm{d}T$ used by Nolet et al. (2006), which in turn were based on anharmonic derivatives for mantle rock by Wentzcovitch et al. (2004), Karato (1993), Karki et al. (1999) and Aizawa et al. (2004). The temperature derivative for postperovskite is unknown, we adopted a ±1% scale in the D" layer (Figs. S10,S20). We do not pretend that this transforms the velocity images into reliable temperature plots, since the derivatives are uncertain (certainly near the CMB) and ΔV_P is also influenced by compositional variations. The reason to vary the scale is to optimize the visibility of anomalies at each depth. We also scale the size of the figure to the true size at the depth of the plot, as indicated in km in the captions.

Figs. S11-S20: As Figs. 1-10, but centered on 0°E.

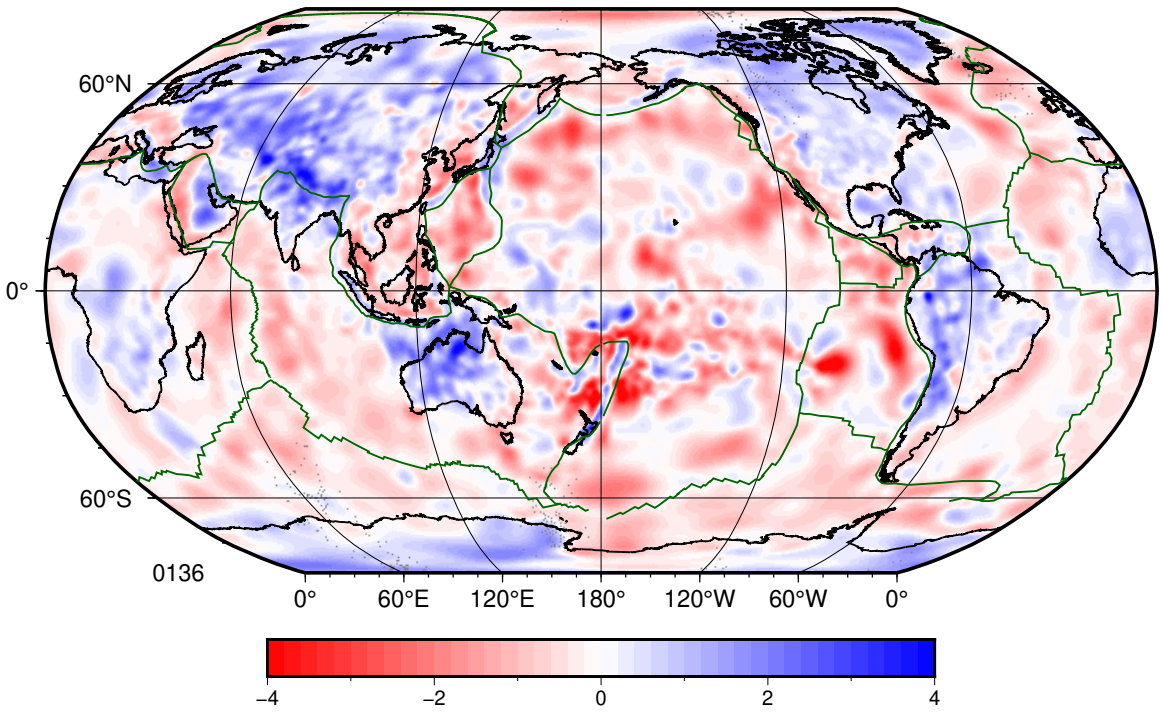

Depth 136 km.

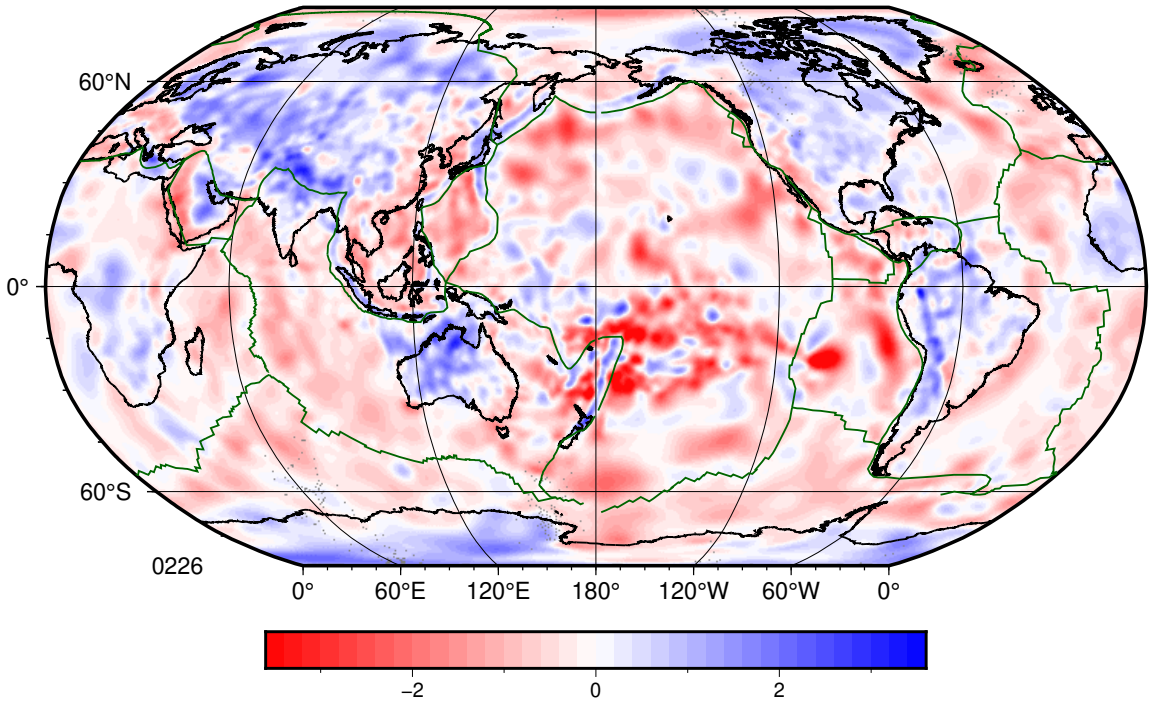

Depth 226 km.

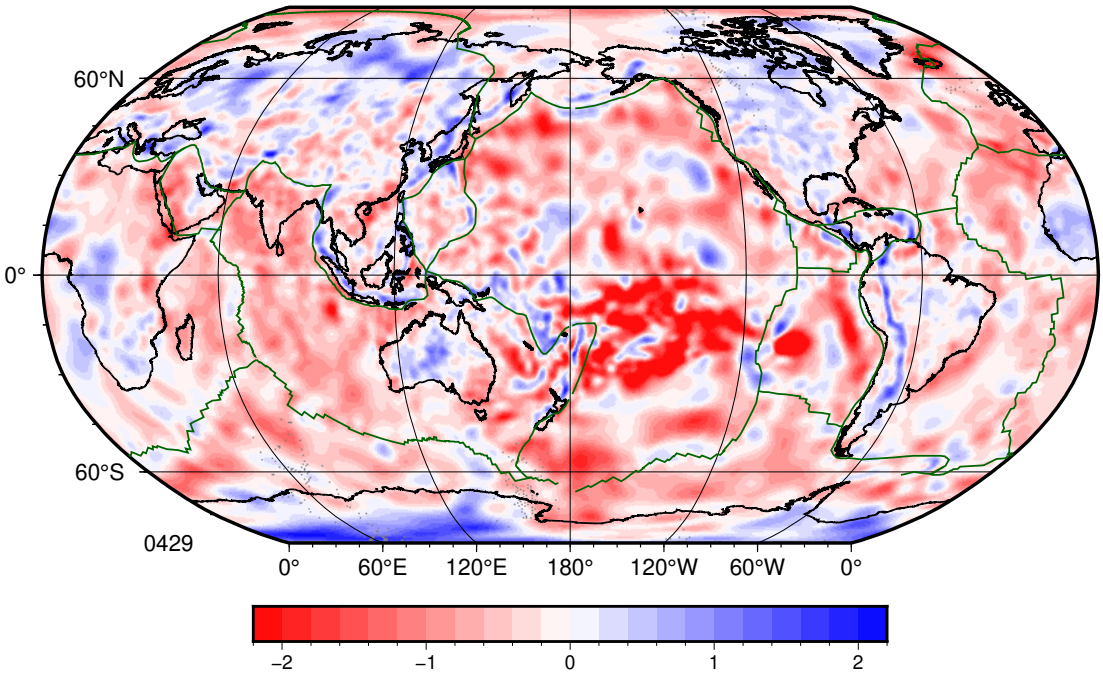

Depth 429 km.

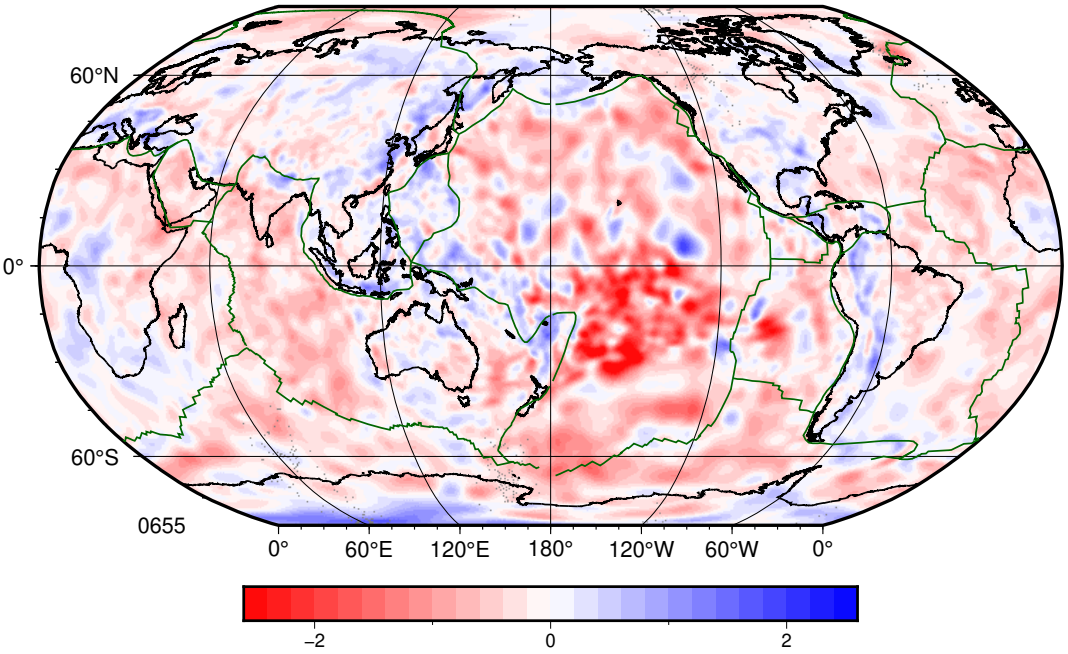

Depth 655 km.

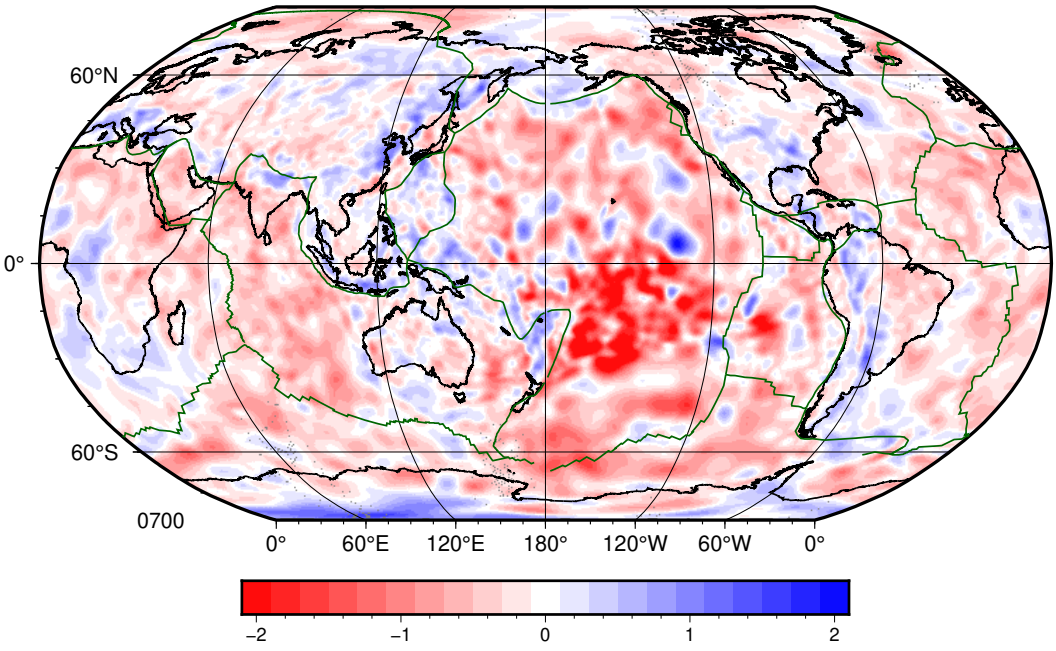

Depth 700 km.

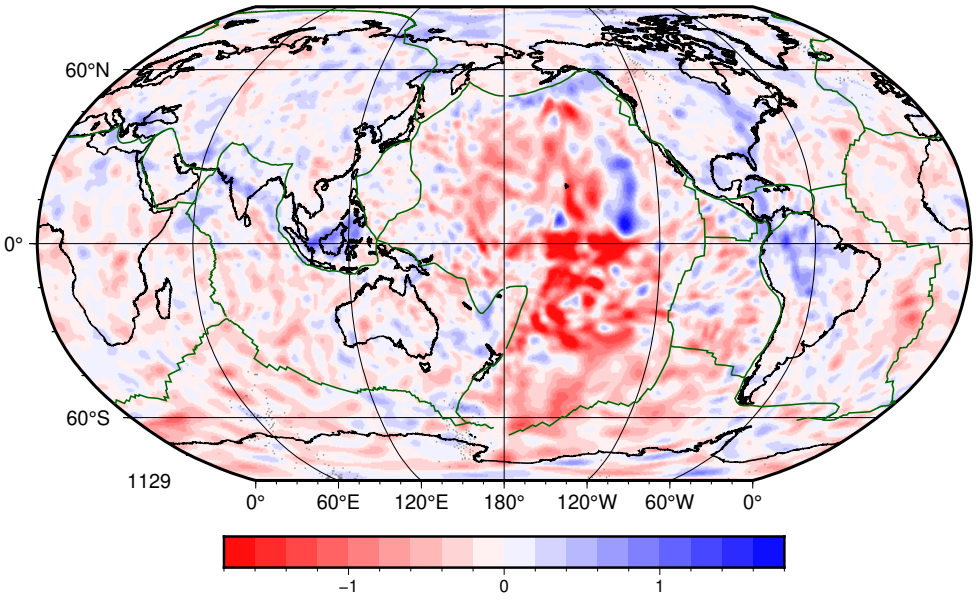

Depth 1129 km.

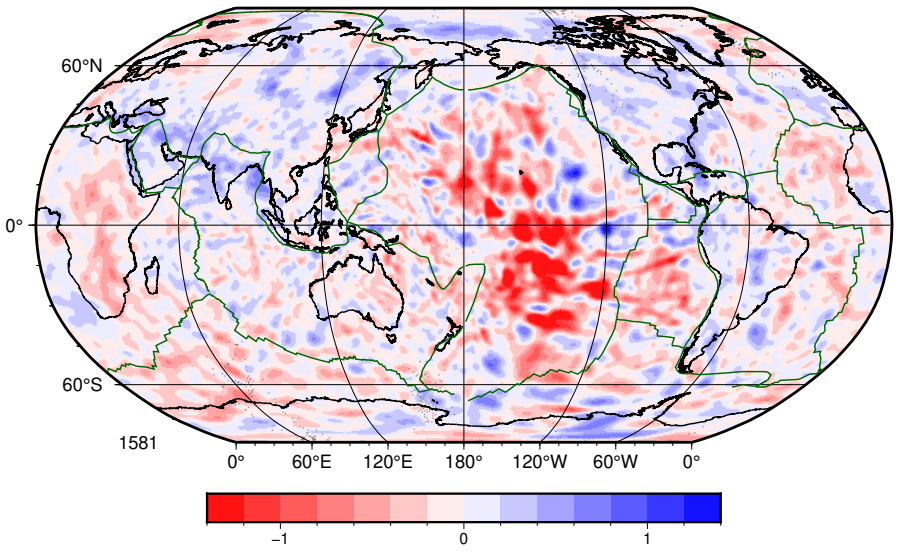

Depth 1581 km.

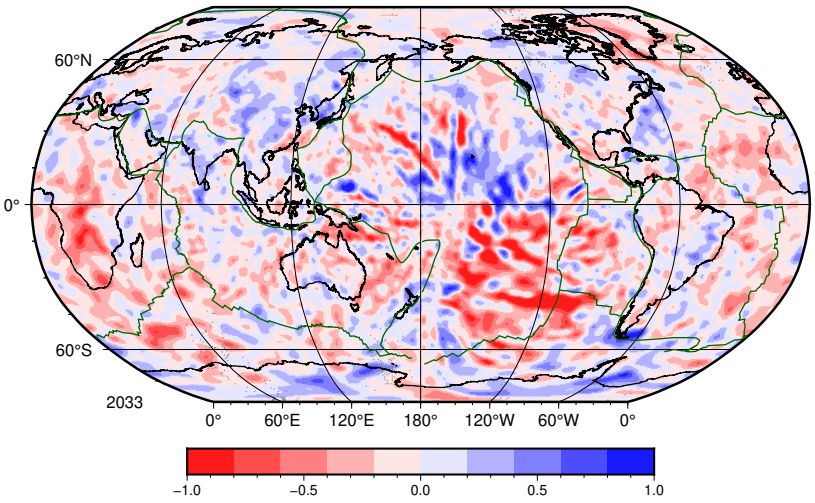

Depth 2033 km.

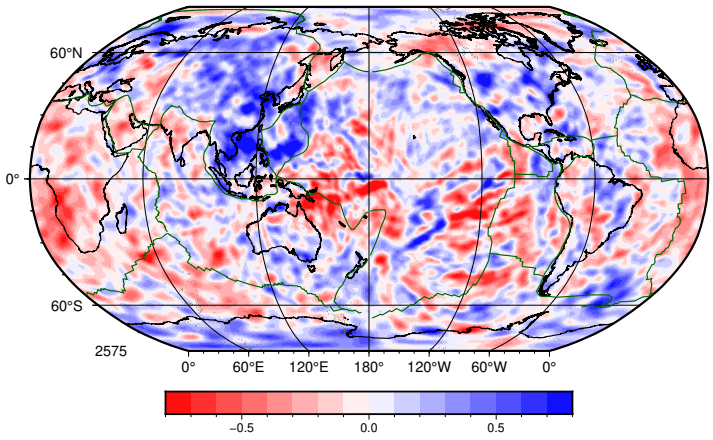

Depth 2575 km.

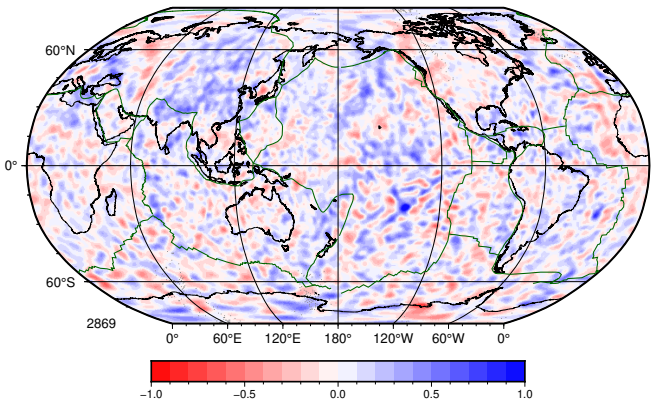

Depth 2869 km.

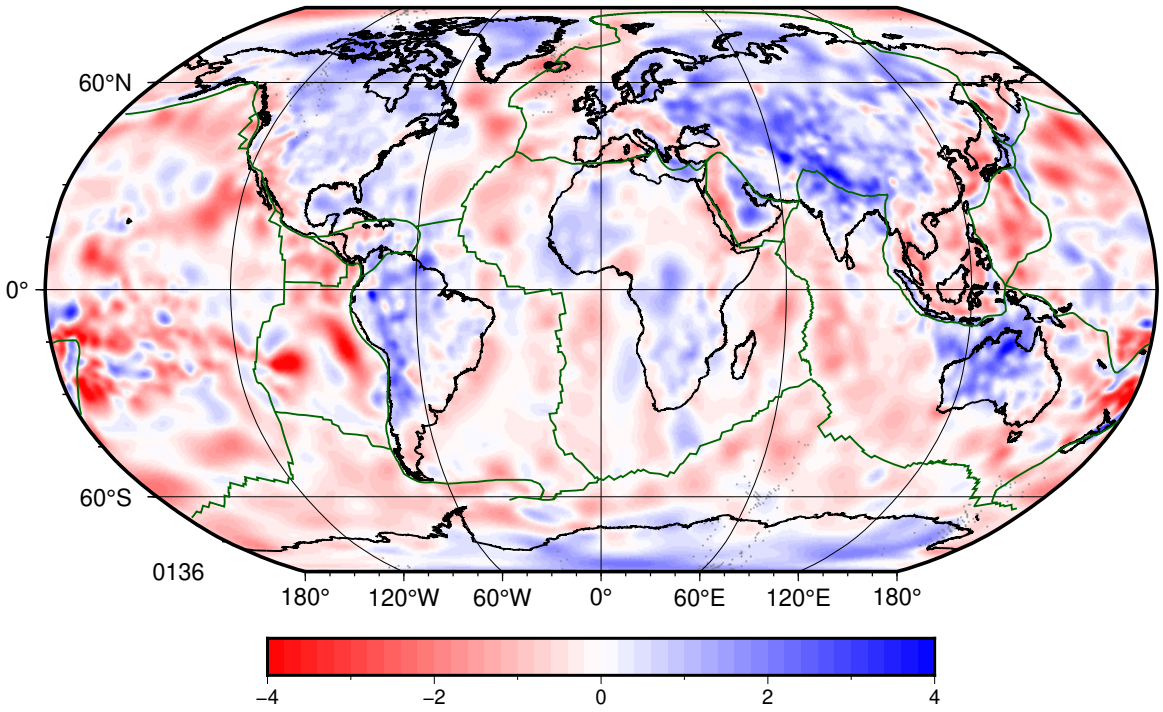

Depth 136 km.

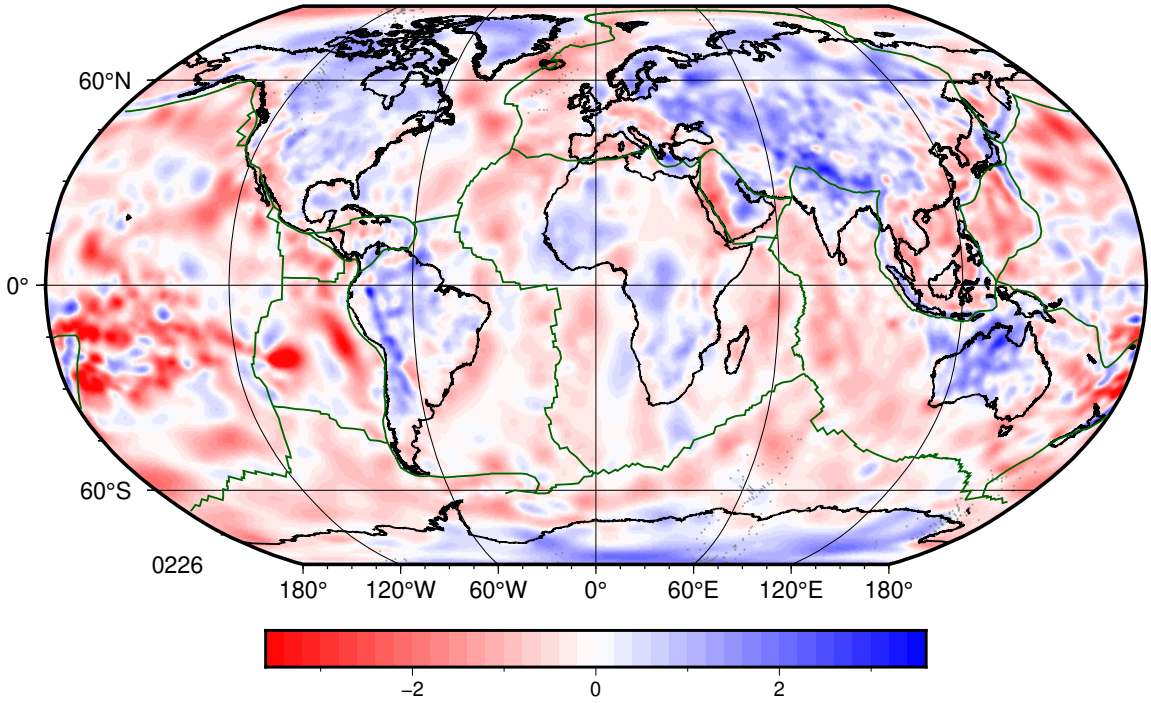

Depth 226 km.

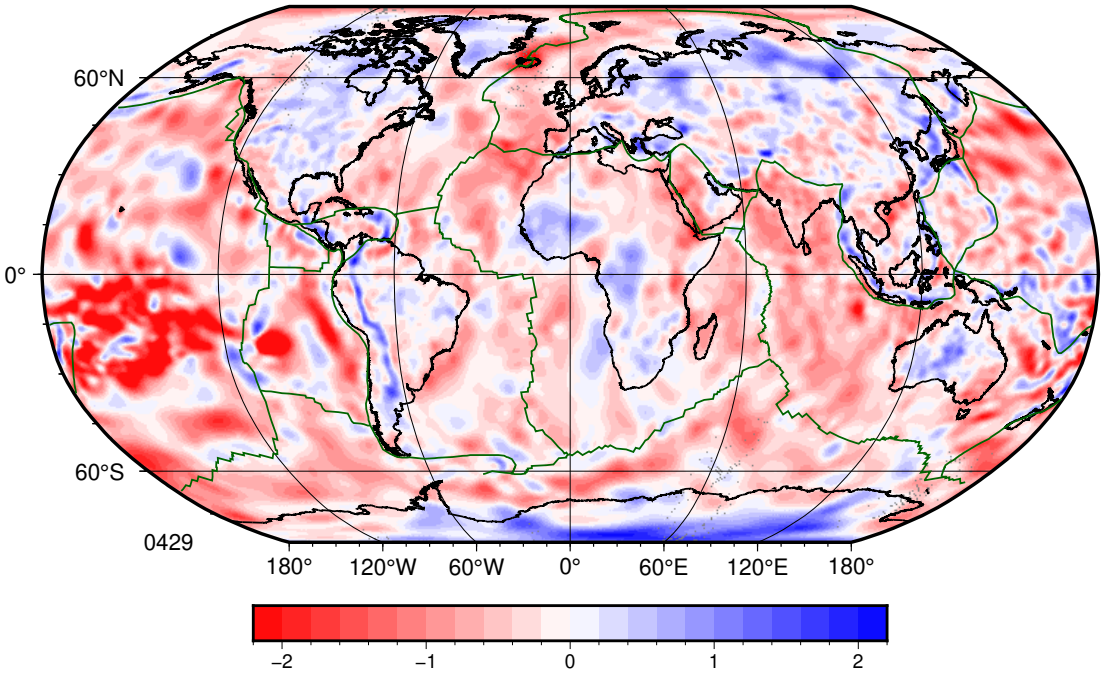

Depth 429 km.

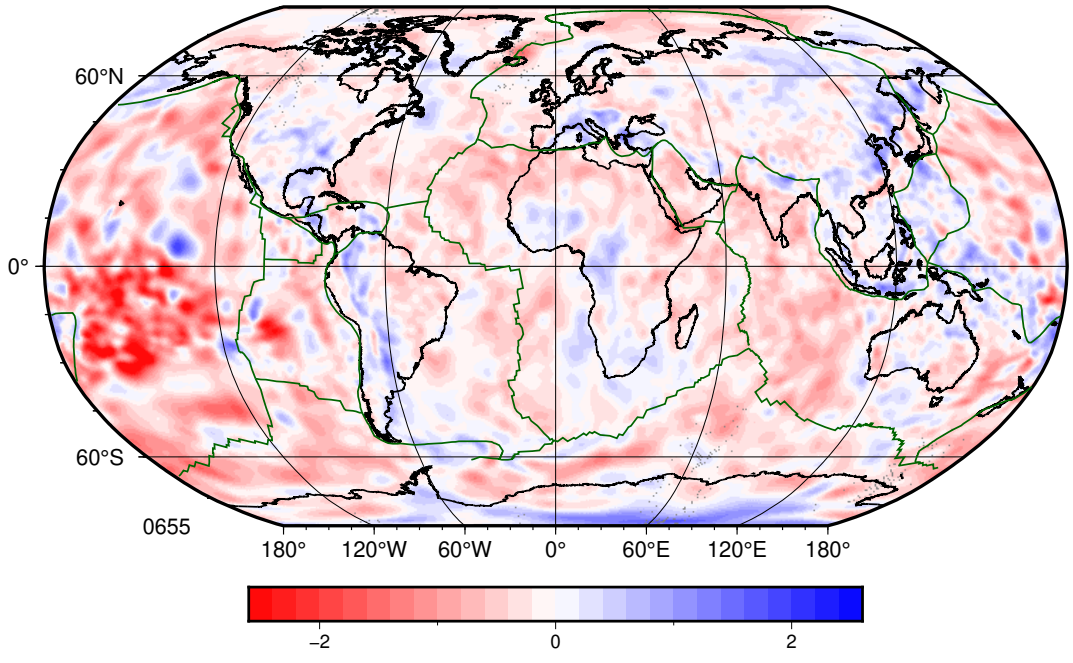

Depth 655 km.

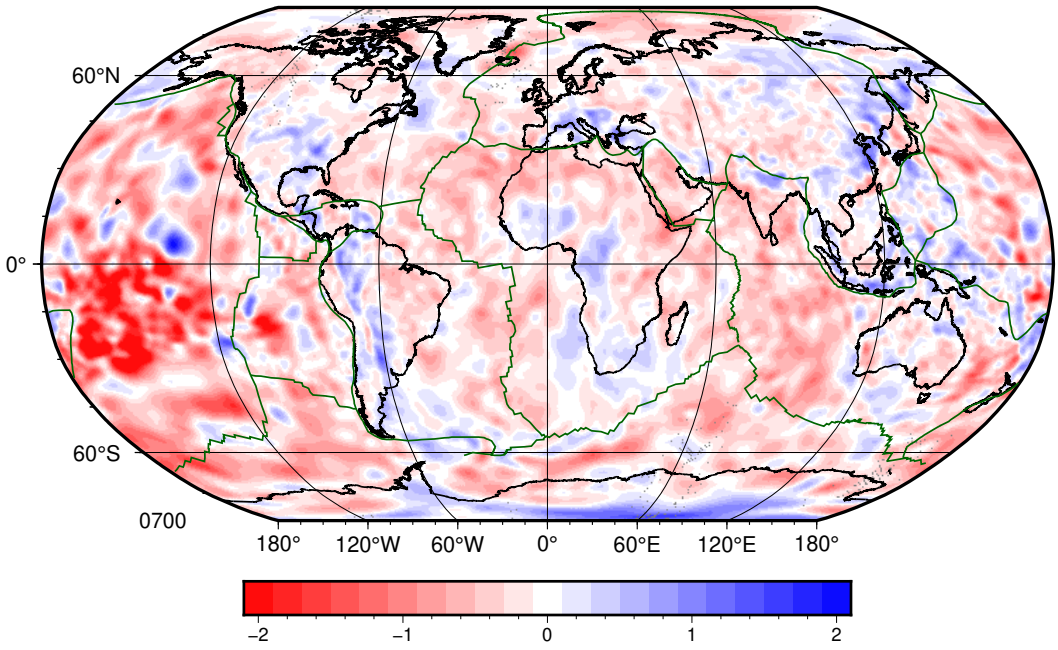

Depth 700 km.

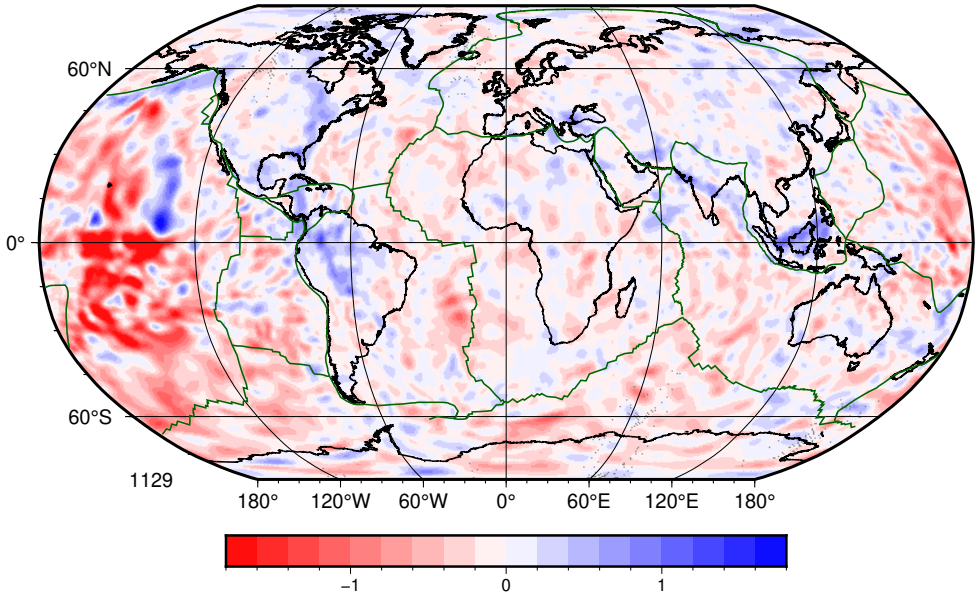

Depth 1129 km.

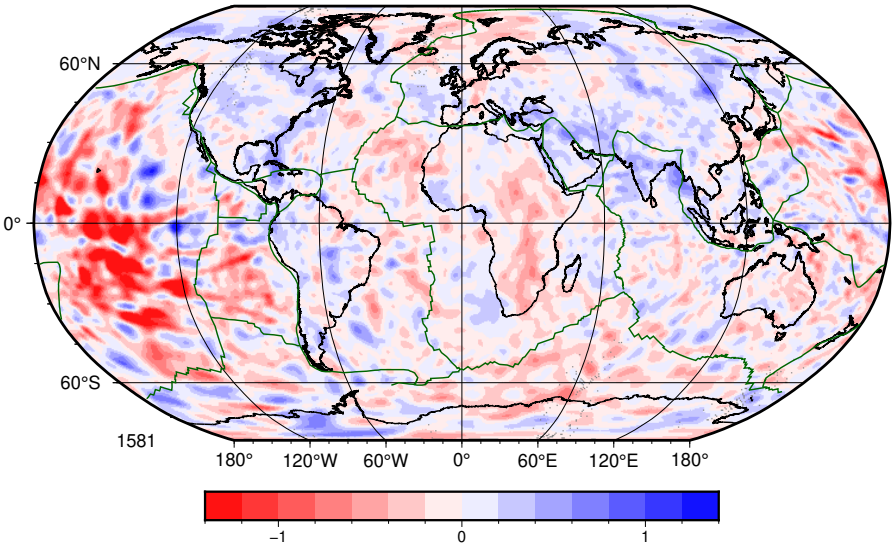

Depth 1581 km.

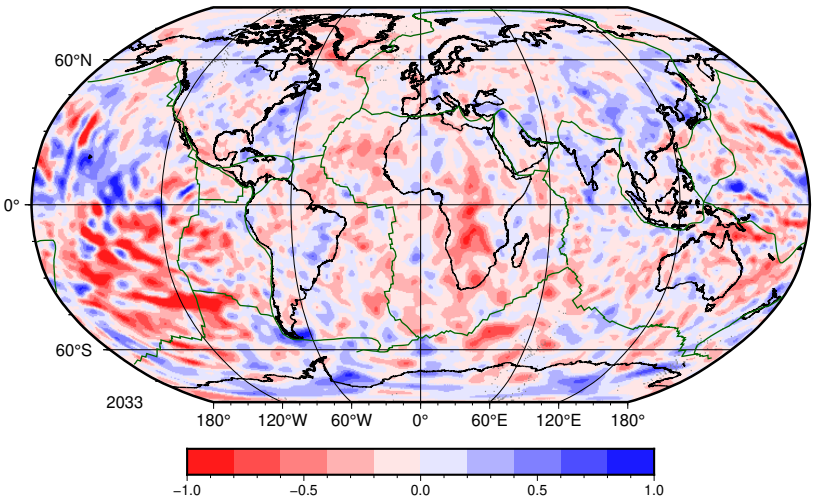

Depth 2033 km.

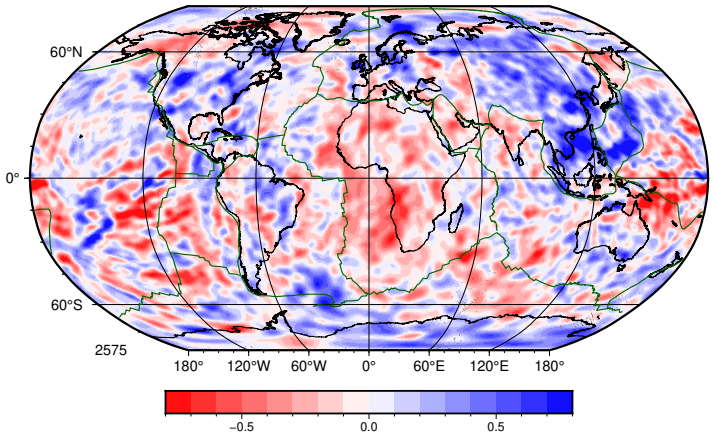

Depth 2575 km.

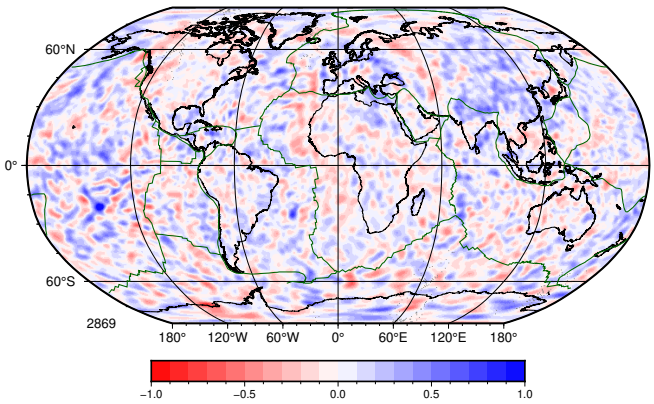

Depth 2869 km.

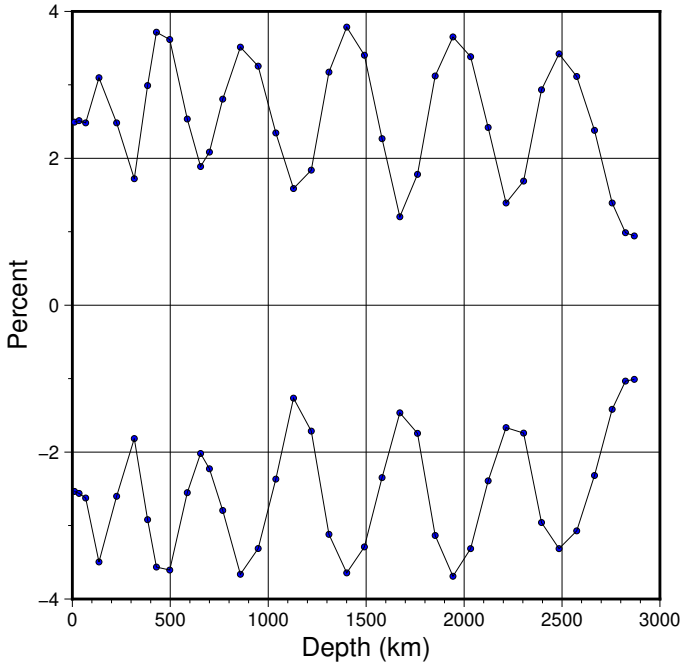

Figure S21: Minimum and maximum anomaly as a function of depth found in the results of the resolution test with 250 km Gaussian spheres. The input spheres had a maximum anomaly of 4%, showing a slight loss of amplitude (for the best resolved areas) that is mostly constant in the lower mantle near 3.5%, except near the very deepest level and near the surface.

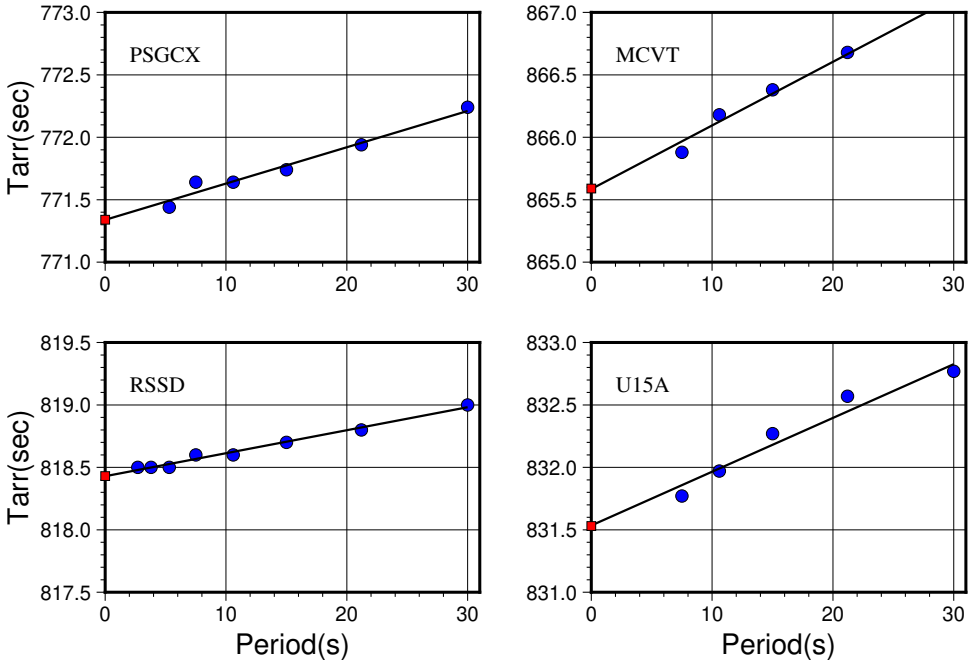

Figure S22: Examples of accepted linear fits to P diffracted dispersion for four different events in four different stations, showing different qualities of fit. Blue dots indicate observed arrival time. A regression algorithm, taking into account the formal errors of each measurement, is used to model the dispersion with a linear fit, which is sampled at zero period (red square).

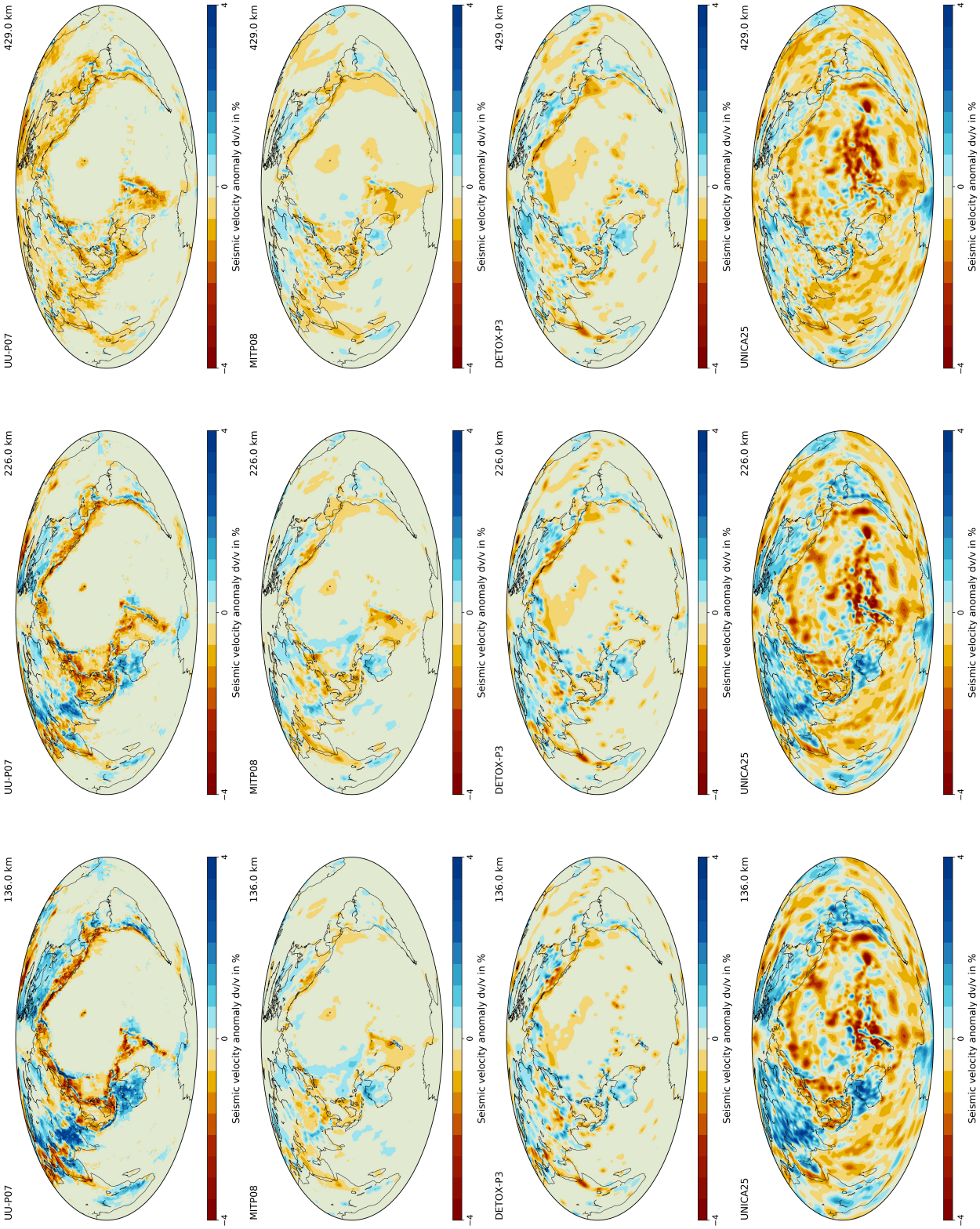

Figure S23: Comparison of Models UU-P07, MITP08, DETOX-P3 with UNICA25. This plot was generated by Submachine (Hosseini et al., 2018).

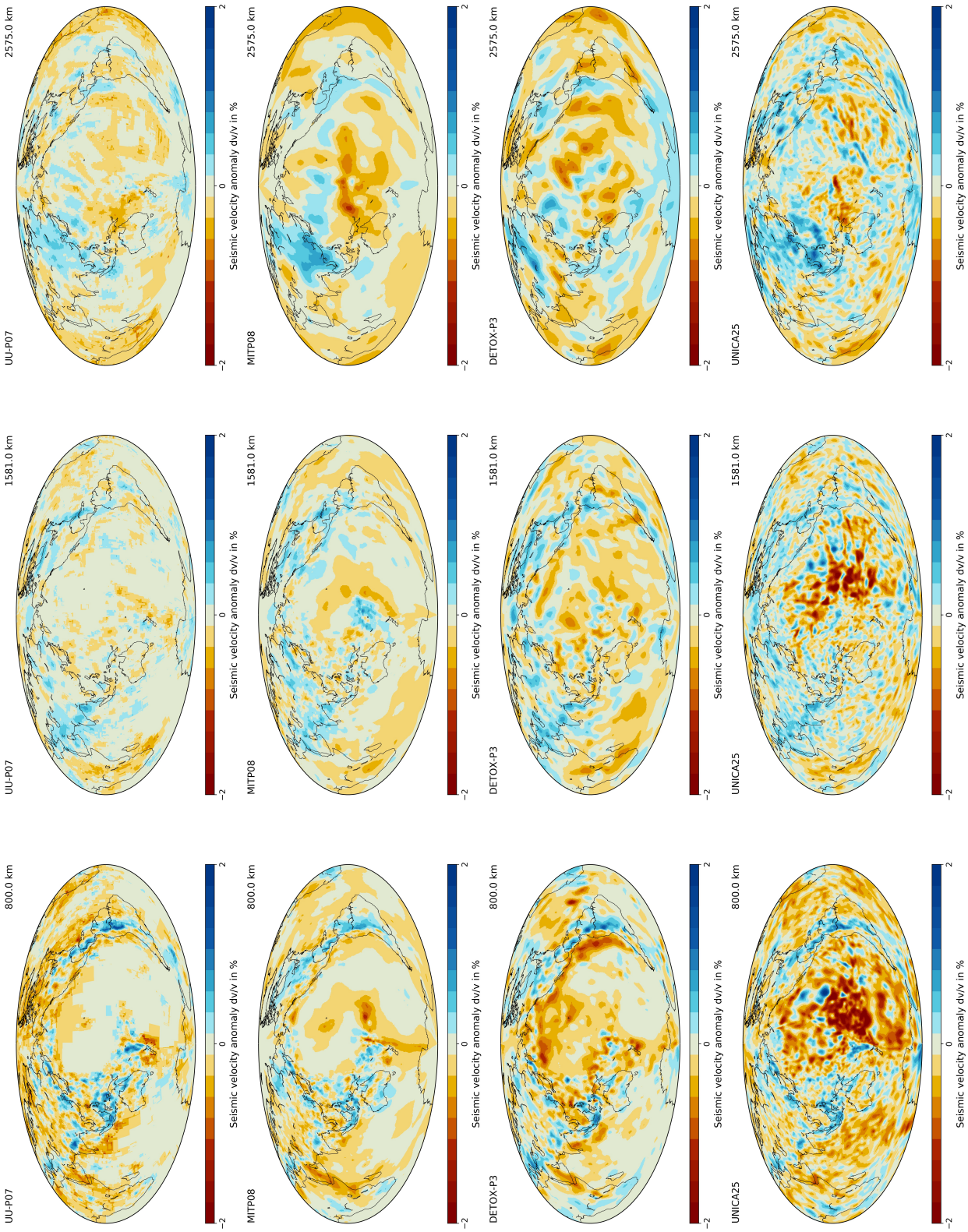

Figure S24: Comparison of Models UU-P07, MITP08, DETOX-P3 with UNICA25. This plot was generated by Submachine (Hosseini et al., 2018).

References

[1] Y. Aizawa, A. Yoneda, T. Katsura, E. Ito, T. Saito, and I. Suzuki. Temperature derivatives of elastic moduli of $MgSiO_3$ perovskite. *Geophys. Res. Lett.*, 31:L01602, 2004.

[2] K. Hosseini, K.J. Matthews, K. Sigloch, G.E. Shepard, M. Domeier, and M. Tseknistrenko. Submachine: Web-based tools for exploring seismic tomography and other models of Earths deep interior. *Geochem. Geophys. Geosys.*, 19, 2018.

[3] S. Karato. Importance of anelasticity in the interpretation of seismic tomography. *Geophys. Res. Lett.*, 20:1623–1626, 1993.

[4] B.B. Karki, R.M. Wentzcovitch, S. de Gironcoli, and S. Baroni. First principles determination of elastic anistropy and wave velocities of MgO at lower mantle conditions. *Science*, 286:1705–1707, 1999.

[5] G. Nolet, S. Karato, and R. Montelli. Plume fluxes from seismic tomography. *Earth Planet. Sci. Lett.*, 248:685–699, 2006.

[6] R.M. Wentzcovitch, B.B. Karki, M. Cococcioni, and S. de Gironcoli. Thermoelastic properties of $MgSiO_3$-perovskite: insights on the nature of the Earth's lower mantle. *Phys. Rev. Lett.*, 92:018501 1–4, 2004.